Intrinsic Signals from Human Cone Photoreceptors

Kate Grieve and Austin Roorda

Purpose. To develop noninvasive means to relate structure to function in human eyes, the authors investigated intrinsic retinal signals at high resolution using an adaptive optics scanning laser ophthalmoscope (AOSLO).

Methods. The AOSLO was used in dual-wavelength mode to stimulate the retina with 658 nm visible light and simultaneously to image the retina with 840 nm infrared light. Modulation of each laser beam using acousto-optic modulators allowed the integration of complex, patterned stimuli into the projected raster, whose exact locations on the retina were recorded into the movie in real time. Stimulus luminance was 12,000 cd/m^2. Twenty- to 30-second movies were recorded, with stimulation occurring at 5 seconds. Intensity changes in the infrared image in response to the visible stimulus were monitored over time.

Results. In five subjects, results showed a clear increase in infrared light scattering in the stimulated region with respect to its surroundings, reproduced in four subjects across multiple imaging sessions. Signal increase began immediately at the onset of the stimulus, reached a peak 2 to 3 seconds after stimulus onset, and decreased to baseline within 2 to 10 seconds. The magnitude of the increase over the stimulated area varied from 0% to 5% between subjects.

Conclusions. Results suggested that the signal originated in the cone photoreceptors, though not all cones contributed to the same extent. In individual cones, signal increases over 20% were measured. Excessive eye movements and dim images gave insufficient signal to noise. Eight subjects showed spurious results for these reasons and were eliminated from the study. (*Invest Ophthalmol Vis Sci.* 2008;49:713–719) DOI: 10.1167/iovs.07-0837

Intrinsic signals are scattering changes that occur in response to stimulation. Intrinsic retinal signals are measured changes in scattered infrared light in response to a visible light stimulus, and they may provide a noninvasive measure of retinal function. They are analogous to cortical functional imaging, during which scattering changes in the visual cortex are measured in response to a visual stimulus.[1] In contrast to cortical function, where response to stimulation is measured at a location different from that at which stimulation occurs, intrinsic retinal signals are induced and detected in the same region, often at the same lateral location. It is, therefore, necessary to decouple the stimulation and response signals by selectively detecting only the scattered infrared light.

A number of different technologies have been used to observe intrinsic retinal signals, most commonly fundus imaging[2–6] (Tso DY, et al. *IOVS* 2007;48:ARVO E-Abstract 1951) and optical coherence tomography (OCT)[7–9] (Hermann B, et al. *IOVS* 2006;47:ARVO E-Abstract 1672). Various responses have been recorded that may be attributed to the influence of different physiological phenomena, depending on their magnitude, polarity (i.e., increasing or decreasing), and time course. Different recording methods may measure different signals, or a combination of factors may contribute to the signal in each case, depending on the spatial and temporal resolution and even the spatial and temporal coherence of the instrument.[10] Wide-field fundus imaging methods provide lateral localization of the signal but essentially no depth resolution, whereas OCT provides precise depth resolution (down to a few micrometers) and moderate lateral resolution. However, despite the moderate lateral resolution of OCT, eye movements have to date caused a loss of control over the lateral location of signal recording in living eyes. The adaptive optics scanning laser ophthalmoscope (AOSLO) allows precise lateral localization of signal origin and some depth resolution (approximately 150 μm) of the signal because of its confocality,[11] though at lower depth resolution than OCT. The exact origin of the intrinsic signals measured by different methods remains uncertain. Some insight may be gained by attempting high-resolution detection.

The retinal intrinsic signals reported in the literature can generally be divided into slow signals and fast signals. Slow signals, with a typical time course of seconds to minutes, are most likely associated with slow processes such as cell swelling or metabolic and blood flow changes in response to the stimulus and are commonly decreasing signals, of negative polarity, because larger cells or higher blood oxygen contents lead to light absorption and, hence, of less scattering[3–6] (Tso DY, et al. *IOVS* 2007;48:ARVO E-Abstract 1951). Pigment bleaching and regeneration should also be classed as a potential source of a slow signal. Fast signals, with time courses of hundreds of milliseconds, are thought to indicate neural activation because the presence of action potentials and postsynaptic potentials and the swelling and shrinking of neurons during activation cause changes in refractive index and cell volume and, hence, scattering changes. The largest changes seen with OCT are positive in polarity and originate principally from the photoreceptor layer.[7,8] With fundus imaging, however, increases and decreases in scattering have been seen in the same retina at different locations with different time courses.[9] Given that the reported magnitude, polarity, and time course of signals vary with each imaging method used, a number of different phenomena may contribute to the measured signal in each instance.

Although the slow signals have been successfully measured in live humans, fast signals have been recorded only on in vitro animal retina preparations or on anesthetized animals.[9] Inconsistency and lack of repeatability have been reported in studies on live humans (Hermann B, et al. *IOVS* 2006;47:ARVO E-Abstract 1672).[12] A scanning laser ophthalmoscope (SLO) has previously been used to look for intrinsic retinal signals in live humans, but no consistent signal could be detected.[12] At-

From the School of Optometry, University of California, Berkeley, California.

Supported by National Institutes of Health Bioengineering Research Partnership Grant EY014375 and by the National Science Foundation Science and Technology Center for Adaptive Optics, managed by the University of California at Santa Cruz under cooperative agreement AST-9876783.

Submitted for publication July 5, 2007; revised September 11, 2007; accepted December 18, 2007.

Disclosure: **K. Grieve**, None; **A. Roorda**, P

The publication costs of this article were defrayed in part by page charge payment. This article must therefore be marked "*advertisement*" in accordance with 18 U.S.C. §1734 solely to indicate this fact.

Corresponding author: Austin Roorda, School of Optometry, University of California, Berkeley, CA 94720-2020; aroorda@berkeley.edu.

tempts to use OCT to measure retinal intrinsic signals in live humans are affected by eye movement artifacts (Hermann B, et al. *IOVS* 2006;47:ARVO E-Abstract 1672).

In this study, we measured intrinsic retinal signals in the living human eye with the AOSLO, which is well adapted to the purpose because of its high lateral and relatively high axial resolution[13] and its stimulus delivery method.[14] In particular, the simultaneous and coincident imaging and stimulation capacity of the multiple-wavelength AOSLO operating in dual-frame mode provides a method of precise stimulus delivery to small retinal areas and quasi-simultaneous, though temporally and chromatically decoupled, detection of the response signal.[15] However, one limitation of our technique was that it was not sensitive to changes on time scales faster than the frame rate. In other words, it was only sensitive to changes on time scales of tens of milliseconds and longer, possibly hindering our ability to detect the fastest intrinsic signals. We sought to vary parameters such as stimulus luminance, form, depth location, and retinal eccentricity to gain information on the signal origin.

Methods

We used the AOSLO[13] in dual-frame imaging mode[15] to provide simultaneous visible wavelength stimulation and infrared imaging. Retinal stimulation was performed with 658-nm visible light, and the retina was simultaneously imaged with 840-nm infrared light. An acousto-optic modulator (AOM) controlled each laser beam, switching the illumination beams on and off in synchronization with the raster scanning to construct each frame and allowing complex, patterned stimuli to be integrated into the projected raster. Because the stimulus is an integral component of the illuminating beam, its exact location on the retina is recorded into the movie in real time. The subject sees the 840-nm imaging light as a dim red square, with the 658-nm stimulus appearing as a bright flash coincident with the imaging raster. Although the 840-nm light is visible to the subject, the spectral sensitivity, $V(\lambda)$, of the retina at this wavelength is so low ($V(\lambda) \sim 3.5 \times 10^{-7}$)[16] as to make stimulation effects from the imaging light effectively zero in comparison with the bright 658-nm stimulus. Brightness of the 840-nm imaging light was 0.67 cd/m^2. Following the methods used in Roorda and Williams[17] to calculate wavelength-dependent cone bleaching, the 840-nm imaging light will bleach 0.02% of the pigment. The low spectral sensitivity at 840 nm also implies that the photopigment absorption is very low and that the imaging wavelength will record essentially no changes in reflectance as a function of changes in the concentration of pigment within the cones. Therefore, the intrinsic signals we observed were not confounded by changes in absorption of the photopigments caused by photobleaching with the 658-nm stimulus. All retinal exposures used in these experiments were at least 10 times below the published maximum permissible exposure limits.[18]

A 3°-square field, the largest field size available for the AOSLO, was used to minimize the relative importance of eye movements and to cover the largest possible area of retina and, hence, measure the largest possible signal. Resolution of the cone mosaic, except in the central 0.5° of the fovea, was achieved on all subjects.

Experiments were performed within a 9°-diameter area around the fovea, where the rod-to-cone areal coverage ratio is low,[19] so that rod contribution to signals is small. We could not resolve individual rod photoreceptors with the AOSLO.

We recorded 20- to 30-second movies with stimulation occurring at 5 seconds. Movies were recorded in random order in groups of five trials. The stimulus covered half the field, either in a half-field pattern, covering the top half of the square field, or in a 2 × 2 checkerboard pattern, covering one top and one bottom quadrant. For every five-trial series of movies recorded, a corresponding five-trial control run was performed in which no stimulus was delivered. Analysis of these movies involved two steps. The first step was to generate a movie of difference frames, in which each frame was equal to the difference between that frame and a baseline prestimulus frame (Fig. 1). The location of scattering changes could be directly visualized in these movies. By correlating the stimulus form with each difference frame, the evolution of the correlation coefficient in time could be monitored to show the presence of the stimulus form in the pattern of scattered light and, hence, the time course of the signal. Averaging across multiple frames of the difference movies improved signal to noise and aided in the detection of weak signals (Fig. 2). The second step was to plot the ratio of the average intensity of the stimulated region with that of the nonstimulated region to quantify the magnitude of intensity changes (Fig. 2). Averaging across multiple frames did not change the signal magnitude of these intensity plots. Therefore, a combination of both analyses was beneficial to confirm the detection of weaker signals. Statistical analysis to measure significance of changes consisted of paired *t*-testing between averaged prestimulus and poststimulus data.

Image processing first involved removal of the sinusoidal distortion caused by the raster scanning using custom Matlab software.[20] Within-frame and intraframe image stabilization, accurate to within a single cone photoreceptor, was applied to all movies to remove eye movements.[20,21] Custom programs were then written using Matlab software to perform the analyses specific to this study.

Healthy subjects were recruited as volunteers for the study. Informed consent was obtained from the subjects after we explained the nature and possible complications of the experiment. Our protocol was approved by the University of California, Berkeley Committee for the Protection of Human Subjects. Imaging on human subjects was conducted according to the principles expressed in the Declaration of

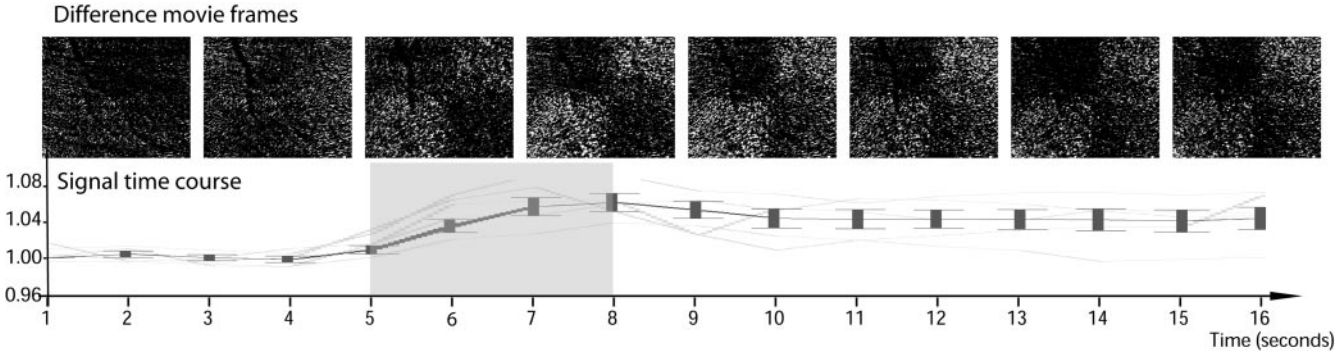

Figure 1. Frames of a difference movie and time course of signal for subject 5, in whom the stimulus was a 2 × 2 checkerboard. Each difference movie image has 30 averaged frames, corresponding to 1 second of imaging. Images at 2, 4, 6, 8, 10, 12, 14, and 16 seconds are shown, and the corresponding signal time course is shown below. The intensity ratio, indicating the percentage intensity change, forms the *y*-axis scale. Error bars are ± SEM. *Solid gray curve*: mean of five trials. *Light gray curve*: individual trial curves.

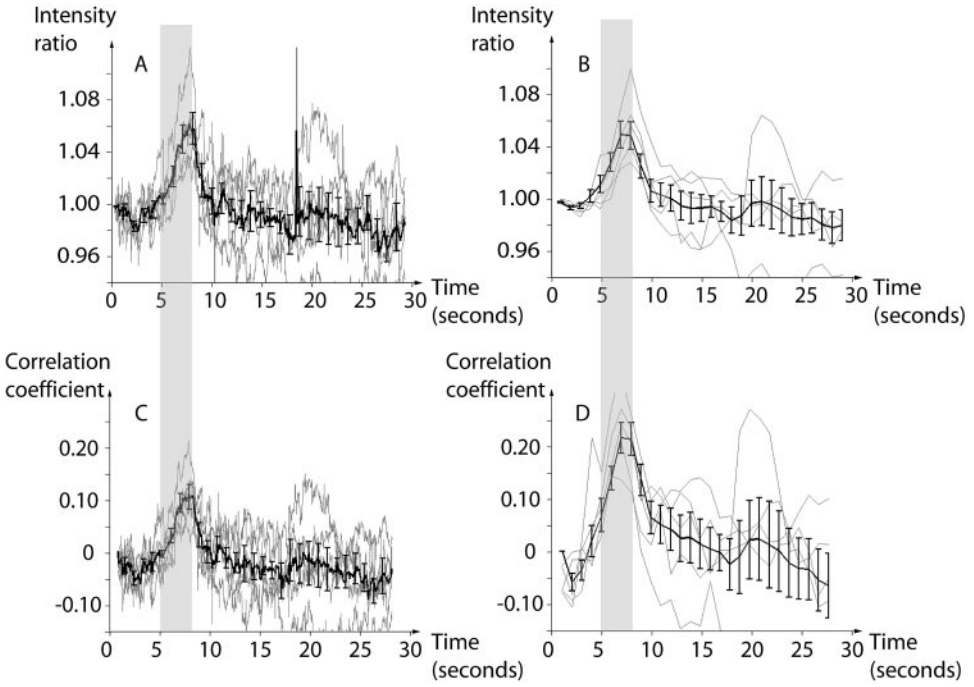

FIGURE 2. Intensity (**A**, **B**) and correlation (**C**, **D**) plots for subject 2 (protocol 1). (**A**, **C**) Time courses of single-frame intensity ratio and correlation, respectively, where each data point corresponds to a 33-ms time interval. (**B**, **D**) Intensity ratio and correlation of 30 averaged frames, corresponding to 1-second intervals. *Dark gray lines*: average of five trials. *Light gray lines*: individual trials. Error bars are ± SEM across the five trials. Although averaging 30 frames reduced noise on curves of the intensity ratio and correlation coefficient, the correlation also improved considerably because of averaging, whereas the intensity ratio did not change in magnitude with averaging.

Helsinki. Patients were aligned and stabilized in the system using a dental impression plate mounted on x-y-z translation stages. Each pupil was dilated with one drop of 2.5% phenylephrine hydrochloride and cyclopleged with one drop of 1% tropicamide.

The subject fixated on an edge of the raster or on a dim laser fixation spot located 3° from the center of the AOSLO scanning beam. Infrared light was used for wavefront sensing and correction over a 5.81-mm pupil. The wavefront sensor measured the subject's refractive error, which was best corrected with trial lenses before wavefront correction by the deformable mirror. After a few iterations of the closed adaptive optics loop, the best correction was reached and fixed to give static correction during movie capture.

RESULTS

Fifteen subjects were imaged, and four of these 15 were imaged on multiple occasions. In all four subjects imaged on multiple occasions, we measured a consistent signal. Signals were also detected in one additional subject who was imaged on a single occasion. Of the 10 remaining subjects, eight were eliminated from the study because of noisy data, and in two no response was measured. Preliminary experiments (protocol 1), carried out on two subjects, aimed to discover the stimulus parameters that would give the most robust response, in terms of stimulus strength, dark- versus light-adapted retina, stimulus form, and fixation location. Once these parameters were fixed, we conducted a series of identical experiments (protocol 2) on the larger group of subjects to investigate reproducibility of the signal.

Testing Stimulus Parameters: Protocol 1

Experiments to investigate the influence of stimulus strength were conducted on two subjects, using a half-field stimulus in a foveal fixation location: the field stretched from the central fovea on the center right-hand side of the field to 3° temporal on the left-hand side. Stimulation was at 30 Hz (i.e., equal to our frame rate) so that it appeared nearly constant to the subject. Stimulus duration was set at 2 to 3 seconds because this appeared to give the most robust response.

The influence of stimulus luminance was investigated in one subject. The power of the red diode laser was varied by placing a neutral density filter wheel in the beam, varying the current delivered by the diode driver, or a combination of the two. This allowed us to vary luminance from 11.5 cd/m^2 to 12,600 cd/m^2. Response was most consistently observed at high luminance values. Within a brightness range from 1500 cd/m^2 to 12,600 cd/m^2, increasing stimulus luminance did not significantly increase response magnitude. The time course remained similar across all experiments.

To obtain the most robust response possible, subsequent experiments were performed at a luminance of 12,000 cd/m^2, or 400 cd · s/m^2 per frame. This bleached 63% of L-cone pigment and 10% of M-cone pigment over 2 seconds of stimulation. Background luminance attributed to scattering in the AOSLO depended on whether the AOM controlling the 658-nm laser was digital or analog. Our analog AOM controller allows more light to leak through than does the digital AOM driver. In the analog controller, background luminance was 58 cd/m^2. According to calculations,[17] this bleaches 1% of L-cone photograph pigment and 0.1% of M-cone pigment before the stimulus. Using the digital AOM driver, background luminance was reduced to 17 cd/m^2. This bleaches 0.4% of L-cone photograph pigment and 0.04% of M-cone pigment before stimulation. The digital AOM driver was, therefore, used when possible to minimize background luminance.

Identical experiments performed on dark- and light-adapted retinas of two subjects showed mixed results, with the dark-adapted retina occasionally generating a higher intrinsic signal. To obtain the most robust response possible, experiments were performed on retinas that had been dark adapted for a 3-minute period before stimulation so that cones could recover from bleaching before the next measurement.

In these preliminary experiments, repeatable responses were seen on multiple occasions on the two subjects according to a protocol we refer to as protocol 1: a series of 30-second long movies was recorded with stimulation occurring at 5 seconds, and stimulation was provided by a 3-second duration, 12,000 cd/m^2, 30 Hz quasi-continuous stimulus, of half-field form, with fixation on the raster edge so that the field stretched

from the central fovea to 3° peripheral. An increase in scattered infrared light was measured in response to the stimulus, of mean magnitude 5% ± 2% across the stimulated area on multiple sessions on the two subjects. IR scatter began to increase at the onset of the stimulus, rose to a maximum at 2 to 4 seconds, remained at a maximum for 1 to 2 seconds, and decreased to baseline in 2 to 20 seconds (Figs. 1, 2). The time to decrease to baseline was the most variable of the time course components between experimental runs.

Noise Sources

Initial experiments to determine the stimulus parameters described (protocol 1) were conducted on two experienced subjects, on whom consistently high-quality images with minimal eye movements could be captured. On imaging-naive subjects, noise in the measurements, principally caused by low image quality and eye movements, became a concern. In particular, it was noted that imaging at the fovea produced highly variable results in 10 of 10 subjects imaged at this location. In addition, the use of a half-field stimulus contributed further to the creation of spurious results. We attributed the noise problems at the fovea to the influence of the specular reflection from the foveal pit, which moved independently from the cone mosaic image and could produce intensity changes not correlated with the stimulus. Six of eight of those subjects rejected for noise had been imaged at the fovea and stimulated with a half-field. Reasons for rejecting the remaining two subjects were excessive blinking in one and accommodation despite tropicamide administration in the other. For our subsequent series of experiments on multiple subjects (protocol 2), stimulation was performed with a 2 × 2 checkerboard at a 3° peripheral (temporal or nasal) location.

Imaging with a Fixed Protocol on Multiple Subjects: Protocol 2

We imaged seven subjects with a fixed protocol (which we refer to as protocol 2). A series of 20-second long movies was recorded, with stimulation occurring at 5 seconds. A 2-second duration, 12,600-cd/m^2, 15-Hz flicker stimulus was used, of 2 × 2 checkerboard form at a 3° peripheral location. Three of these seven subjects were imaged on multiple occasions. Of the seven subjects imaged with this protocol, five showed a clear increase in scattered IR light in response to the visible stimulus (magnitude 0.1%–2.2%). Two of the three subjects who were imaged on multiple occasions showed repeatable responses under the same conditions on different occasions. The time course for the signals was similar across all subjects: signal increase began 0 to 2 seconds after stimulus onset, rose to maximum response after 1 to 3 seconds, sustained maximum response for 0 to 5 seconds, and gradually returned to baseline in 2 to 10 seconds. Time to return to baseline was the most variable component of the time course between subjects. In two of seven subjects, we were unable to detect a clear response. These subjects were imaged on one occasion only; hence, reproducibility of the zero response was not tested. Results for the six subjects who had positive responses are shown in Figure 3 and tabulated in Table 1.

Discussion

Signal Origin

Microscopic lateral imaging with adaptive optics makes AOSLO uniquely able to determine, in vivo, the spatial origin of the

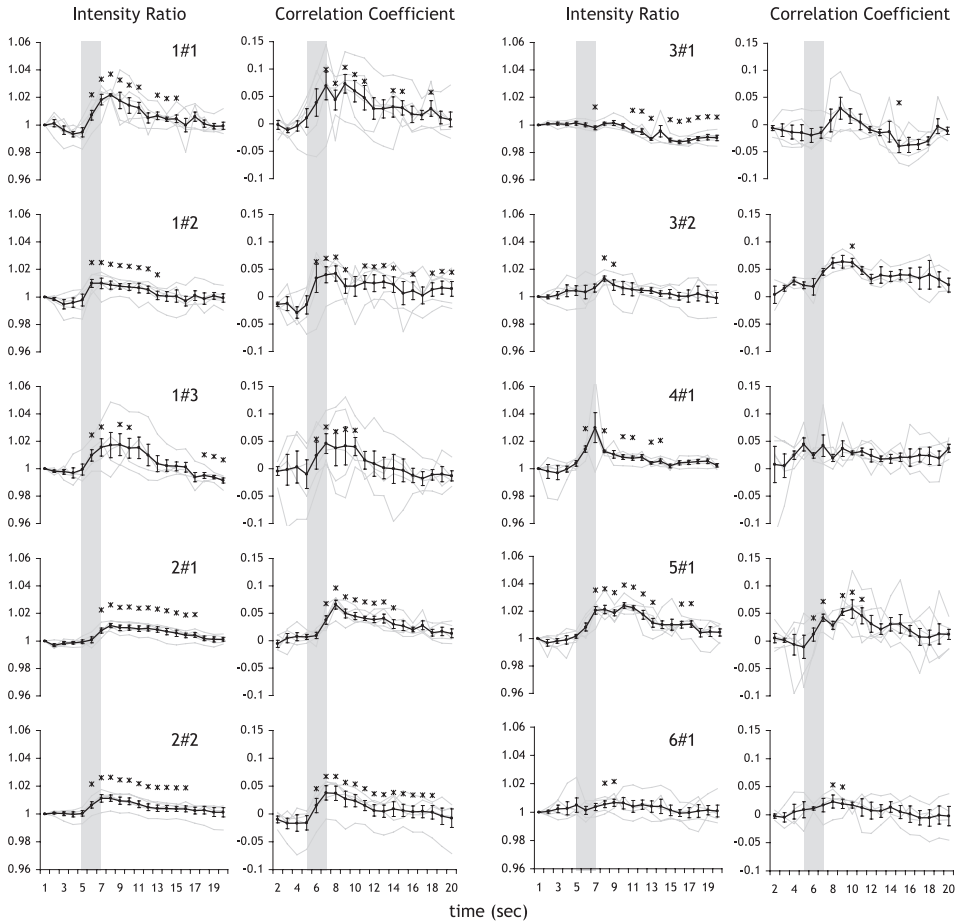

Figure 3. Intensity ratio and correlation coefficient time courses for each experimental run on six subjects (protocol 2). Curves are shown for 30 averaged frames, corresponding to 1-second intervals. *Dark gray lines*: average of all trials. *Light gray lines*: individual trials. Error bars are ± SEM across the trials. *Significant change, calculated by a two-tailed paired *t*-test between data from the 5 seconds prior to the stimulus and each subsequent second. For trial 3#1, the significant values are lower than prestimulus values.

TABLE 1. Summary of Results from Six Subjects under a Fixed Protocol (Protocol 2)

	Peak Signal Magnitude (% ± SE)			Peak Correlation Magnitude ± SE			Time Period of Significant Change (Seconds after Stimulus Onset)		
Subject	**Run 1**	**Run 2**	**Run 3**	**Run 1**	**Run 2**	**Run 3**	**Run 1**	**Run 2**	**Run 3**
1	2.19 ± 0.08	0.99 ± 0.28	1.75 ± 0.80	0.073 ± 0.017	0.042 ± 0.014	0.046 ± 0.018	1–12	1–15	1–5
2	1.12 ± 0.15	1.13 ± 0.24	—	0.066 ± 0.008	0.038 ± 0.012	—	2–12	1–13	—
3	—	1.32 ± 0.19	—	—	0.064 ± 0.011	—	—	3–4	—
4	1.27 ± 0.09	—	—	—	—	—	1–9	—	—
5	2.13 ± 0.31	—	—	0.058 ± 0.016	—	—	2–12	—	—
6	0.66 ± 0.26	—	—	0.023 ± 0.011	—	—	3–4	—	—

Results are the mean of five trials. Error values are the SEM. Time period of significant change is measured in seconds, with time point zero located at stimulus onset.

intrinsic retinal signal. This is accomplished by comparing the spatially resolved poststimulus and prestimulus ratio image, pixel by pixel, with the corresponding intensity image of the cone mosaic. Pixel values in the ratio image, as opposed to a difference image, are independent of the corresponding pixel values in the intensity image; therefore, any correlations between the two images will reveal true functional correlations and not artifacts. Our comparisons of the ratio image to the prestimulated intensity images show that the signal comes primarily from the cones, though not all cones respond equally. Confirmation of the fact that our signal originates from cones is provided by plotting each pixel's intensity values from the intensity image (showing retinal structure) against the corresponding pixel values from the ratio image (showing intrinsic signals; Fig. 4). Pixels of higher intensity in the prestimulated intensity image correspond to cones. If larger intrinsic responses come from the brighter regions of the image, it follows that the intrinsic signals must also originate from the cones or be wave guided through them. This is indeed what we found. The largest signal changes, coming from the individual cones, were approximately 20%. Plotting pixel-by-pixel values rather than cone-by-cone values avoided artifacts that might have been introduced by assumptions made in cone identification.

Sophisticated image stabilization software to remove eye movements was required for our analysis to give valid results because any small error in image stabilization on the single cone scale would generate "cone shadow" artifacts across the ratio image that would outweigh true signal and average changes to zero. Precise image stabilization is especially important in an SLO system, where eye movements cause intraframe distortions and interframe shifts. Our stabilization software corrected the intraframe distortions in narrow horizontal strips and has been demonstrated to correct to a single cone scale.[20,21]

Although the axial resolution of AOSLO is large compared with OCT, we could also determine the axial origin of the intrinsic signal. A confocal pinhole was selected that provided axial resolution of approximately 150 μm. By imposing defocus on the deformable mirror, we stepped through a range of retinal layers with the AOSLO (Fig. 5).[22,23] Movies were re-

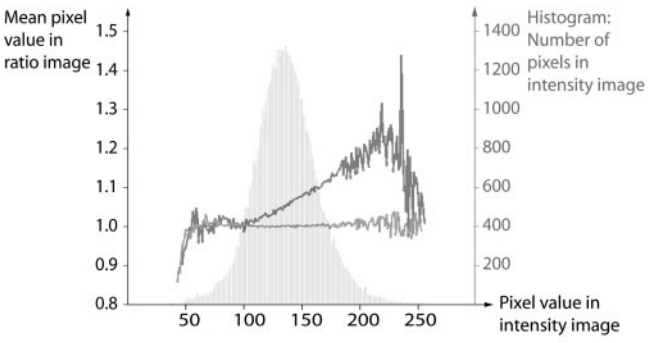

FIGURE 4. Pixel-by-pixel correlation plots and histogram, on subject 2, from a single trial. Pixel values of an intensity image (showing retinal structure) are plotted against corresponding pixel values in a ratio image (i.e., a later frame divided by a prestimulus frame, showing the location of intrinsic signals). *Light gray line*: frame 2 divided by frame 1 (both prestimulus, equivalent to frames 2 and 1 of Fig. 1), where no intrinsic signal is seen. *Dark gray line*: frame 8 divided by frame 1 (poststimulus divided by prestimulus, equivalent to frames 4 and 1 of Fig. 1), where intrinsic signals are present. The positive slope reveals that the brightest pixels (i.e., cones) in the intensity image are also the locations of highest intrinsic response. These curves are plotted from a movie in which frames were averaged in groups of 30, corresponding to 1-second intervals. The background plot is a histogram showing the distribution of pixel values in the prestimulated intensity image.

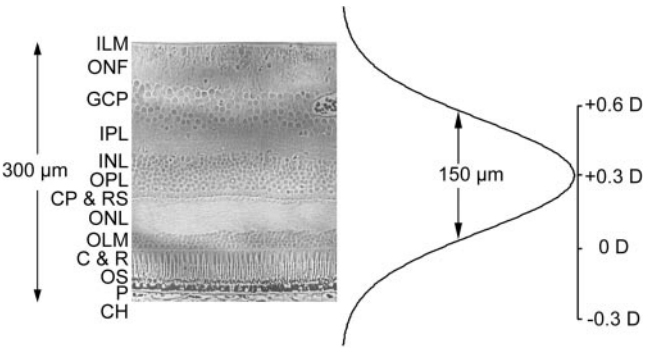

FIGURE 5. Illustration of axial resolution of the AOSLO in relation to retinal thickness. On the *left* is a histologic cross-section of the human retina, reproduced with permission from Boycott BB, Dowling JE. Organization of the primate retina: light microscopy. *Philos Trans R Soc Lond B Biol Sci*. 1969;255:109–184. ILM, inner limiting membrane; ONF, optic nerve fiber layer; GCP, ganglion cell perikarya; IPL, inner plexiform layer; INL, inner nuclear layer; OPL, outer plexiform layer; CP & RS, cone pedicles and rod spherules; ONL, outer nuclear layer; OLM, outer limiting membrane; C & R, inner segments of cones and rods; OS, outer segments of cones and rods; P, pigment epithelium; CH, choroid. The normal human retina is approximately 300 μm thick at the location of imaging.[23] On the *right* is a Gaussian curve showing the axial resolution of the AOSLO.[11] Scale bar indicates the central positions of this Gaussian profile in diopters of mirror defocus, when focused on four different retinal layers. All retinal tissues contained within the axial resolution profile may contribute to the signal wave guided through the cones and detected at the cone tips, with their relative contributions weighted by the Gaussian profile.

TABLE 2. Results of Retinal Layer Imaging in Two Subjects

	Subject 3		Subject 5	
Focal Position (D)	Intensity Change (%)	Correlation	Intensity Change (%)	Correlation
+0.6	1.0 ± 0.2	0.01 ± 0.01	0.6 ± 1.4	0.00 ± 0.06
+0.3	0.9 ± 0.3	0.05 ± 0.01	1.2 ± 0.2	0.04 ± 0.01
0.0	1.4 ± 0.2	0.06 ± 0.01	1.7 ± 0.3	0.09 ± 0.03
−0.3	0.6 ± 0.1	0.04 ± 0.01	N/A	N/A

The defocus imposed on the deformable mirror, measured in diopters, allowed us to focus on the nerve fiber layer (+0.6 D), in the inner retinal layers (+0.3 D), on the photoreceptors (0 D), and in the choroid (−0.3 D). Results are the mean of five trials. Error values are the SEM.

corded with best focus on the photoreceptors, below the photoreceptors extending into the choroid, above the photoreceptors on the inner retinal layers, and on the nerve fiber layer. Table 2 shows the results. In 2 of 2 subjects, the change in intensity ratio was highest at the plane of best focus on the photoreceptors.

The signal we detected represented the total percentage reflectance change integrated within the axial resolution profile illustrated in Figure 5. Our results have polarity and time courses similar to those measured with OCT, but the magnitudes are different. However, the differences between AOSLO and OCT intrinsic signal magnitudes are attributed not only to differences in axial resolution but also to the different mechanisms by which the scattered signal was recorded. An AOSLO images features in the retina by raster scanning a focused spot on the retina, which is imaged again though a confocal pinhole. Axial and lateral image resolution is limited by diffraction, whereas OCT axial resolution is limited by the coherence length of the light source. The important difference occurs with the photoreceptors, where the light is wave guided and emerges from the inner segments at the location of the external limiting membrane. Although little light actually scatters from that layer, the AOSLO signal detects the combination of all wave-guided reflections as though they are originating from that surface. OCT reveals that the sources of wave-guided light originate from the inner/outer segment junction and from the outermost tip of the outer segment (Gao W, et al. *IOVS* 2007; 48:ARVO E-Abstract 3849). Therefore, the intensity of photoreceptors in the AOSLO image is a sum of the signal from the outer segments, the inner-outer segment junction, and the inner segment tips. The AOSLO axial section also includes scattered light from every other layer that falls under the axial resolution profile, such as the outer nuclear layers, the retinal pigment epithelium, and the choroid, where signal decreases may occur because of blood flow contributions, but these are weighted by the axial resolution profile (Fig. 5). As such, we expected our changes to be smaller than those of OCT because our changes combined sources with negative and positive intrinsic signals and were measured relative to the intensity of prestimulated images that integrate reflectance from a much thicker axial section, much of which has no intrinsic signal.

With the use of OCT in excised rabbit retina, Bizheva et al.[7] found positive intrinsic signals of up to 80% over a time course of seconds originating in the outer segments and negative intrinsic signals of 30% with a similar time course in the inner segments, for a combined change of approximately 50%. OCT in living rat found an approximately 25% near infrared reflectance increase in response to visible light stimulation that was largely confined to the outer segment.[8] OCT measurements of the intrinsic signal magnitude, integrated over the whole photoreceptor, were up to one order of magnitude higher than our results, with the same polarity and similar time course. Compared with results obtained with fundus imaging (Tso DY, et al. *IOVS* 2007;48:ARVO E-Abstract 1951),[2–6] our signals are almost one order of magnitude larger and are of opposite polarity, though of similar time course. Recent studies have shown that the negative polarity signals detected with fundus imaging methods result from blood flow in the choroid (Tso DY, et al. IOVS 2007;48:ARVO E-Abstract 1951). In fundus imaging systems with no depth discrimination, the negative choroidal blood flow signal combines with the positive retinal signal, most often yielding small negative responses but sometimes also yielding positive responses.[2,6] Because of the depth resolution of AOSLO, our results tend to agree more with those obtained with OCT[7,8] than with fundus imaging.

The correlation of the signal with the stimulus form was highest in the photoreceptors and decreased at other layers, even though an intrinsic signal was present (Table 2). This confirms the notion that the signal is initiated by the excitation of the light-sensitive photoreceptors, where the response will necessarily correlate with the stimulus pattern. By the time the visual signals activate various other neural layers, some of the retinotopy will be lost, and the consequent spatial correlation with the stimulus will decrease. With OCT, signals have also been detected in upper retinal layers in in vitro rabbit retina, particularly the inner plexiform layer, where a signal increase of approximately 25% was seen, though with a slower rise to maximum response (5 seconds).[7]

It has been suggested that the origin of the retinal intrinsic signal could be ion flux, cell swelling and shrinking, membrane hyperpolarization, or structural changes in the outer segment disks, though many of these factors are known to occur on a time scale shorter than that of the observed signals.[9] Our results (Fig. 2) demonstrated that the increased scatter occurred within the cone and not between the cones. An unexpected advantage of this finding is that the contrast of the cone mosaic is actually increased by the presence of an intrinsic signal. However, the origin of the signal in other layers was less well defined; the cells were not visualized by conventional AOSLO because of their relative transparency.

Changes in absorption caused by photobleaching cannot affect the intrinsic signal directly given that the absorption of all the photopigments is essentially zero at the 840-nm imaging wavelength. However, secondary nonabsorptive changes as a result of photobleaching cannot be ruled out. If secondary scattering changes as a result of photobleaching were the source of the signal, we would have expected to detect signal selectively from L-cones because they were preferentially bleached by the stimulus light. Changes in scattering caused by photobleaching were not likely, however, considering the following three observations: intrinsic signals of similar magnitude and time course were observed for dimmer stimuli, where significantly less photobleaching occurred; intrinsic signals often returned to baseline within seconds after the stimulus, whereas the generation of new photopigment after a bleach had a longer time course; the nature of the intrinsic signals we observed was variable between subjects and from day to day in single subjects. Photopigment bleaching and regeneration dynamics, on the other hand, are stable and predictable.[24]

Noise Sources

To calculate the average intensity of the stimulated and unstimulated areas of the image, only the areas common to every frame in the movie after eye movement compensation were included in the calculation. This meant that for subjects with large eye movements, the common area was small so that results became noisy. Subjects with too much eye movement

had to be removed from our study because the signal-to-noise ratio was not adequate. Blinks, causing dark frames, were removed from the analysis; one subject with excessive blinking was rejected from the study. Subjects whose retinas produced consistently low-intensity images had to be excluded because the data were too noisy.

Tear film break-up reduced the intensity of the entire image in our AO system in a uniform way because it introduced new aberrations not compensated by the static AO correction. The intensity ratio method we used to measure intrinsic signals was unaffected by intensity changes that globally affected the entire image, so that the intensity changes we measured could not have resulted from tear film changes. However, lower intensity images were inherently noisier; where possible, we asked subjects to blink and restore a smooth tear film just before stimulus delivery if breakup was observed.

Stimulus form and fixation location appeared to be influencing factors on the noisiness of results. When imaging the fovea, the specular reflection arising from the foveal pit moves differently from retinal structures in the plane of focus and can cause spurious signals to be detected. Noise effects are also aggravated by use of a half-field rather than a checkerboard stimulus. Large eye movements can cause frame edges to become visible in the stabilized movie. Frame edges correlated with a half-field pattern, which caused our correlation coefficient curves to increase erroneously. Therefore, we used a checkerboard-patterned stimulus for most of our measurements because it is unlikely that natural changes occur in a checkerboard pattern, and large eye movements cannot produce checkerboard-shaped artifacts in frames. We also moved fixation to a 3° peripheral location for the fixed protocol experiments (protocol 2) to avoid the foveal pit.

Despite these improvements in experimental protocol, our measurement technique remained sensitive to eye movements and low image quality, which made the signal-to-noise ratio too low for reliable measurement in some subjects. Several measures were taken to reduce this sensitivity to noise, such as stimulus stabilization on the retina. We also hope to improve the temporal resolution of our detection by increasing the frame rate above 30 frames/s (while also decreasing our field size) to detect faster signals (<33 ms).

Conclusion

Unambiguous intrinsic signals were recorded in five of 15 of our subjects. The scattering changes detected were caused by the visible stimulus, as proved by the presence of the stimulus form in the difference images. The response magnitude averaged over the stimulated area increased between 0% and 5% increase, with a time course of seconds. The signal at the cone photoreceptor layer came from the photoreceptors themselves and not the spaces between them. Increased scattering responses from individual cones reached approximately 20%. In our experiments, the most robust responses were measured at a 3° peripheral location with a bright stimulus.

References

1. Grinvald A, Lieke E, Frostig RD, Gilbert CD, Wiesel TN. Functional architecture of cortex revealed by optical imaging of intrinsic signals. *Nature*. 1986;324:361–364.
2. Abràmoff MD, Kwon YH, Ts'o D, et al. Visual stimulus-induced changes in human near-infrared fundus reflectance. *Invest Ophthalmol Vis Sci*. 2006;47:715–721.
3. Tsunoda K, Oguchi Y, Hanazono G, Tanifuji M. Mapping cone- and rod-induced retinal responsiveness in macaque retina by optical imaging. *Invest Ophthalmol Vis Sci*. 2004;45:3820–3826.
4. DeLint PJ, Berendschot TTJM, van de Kraats J, van Norren D. Slow optical changes in human photoreceptors induced by light. *Invest Ophthalmol Vis Sci*. 2000;41:282–289.
5. Nelson DA, Krupsky S, Pollack A, et al. Special report: noninvasive multi-parameter functional optical imaging of the eye. *Ophthalmic Surg Lasers Imaging*. 2005;36:57–66.
6. Hanazono G, Tsunoda K, Shinoda K, Tsubota K, Miyake Y, Tanifuji M. Intrinsic signal imaging in macaque retina reveals different types of flash-induced light reflectance changes of different origins. *Invest Ophthalmol Vis Sci*. 2007;48:2903–2912.
7. Bizheva K, Pflug R, Hermann B, et al. Optophysiology: depth-resolved probing of retinal physiology with functional ultrahigh-resolution optical coherence tomography. *Proc Natl Acad Sci USA*. 2006;103:5066–5071.
8. Srinivasan VJ, Wojtkowski M, Fujimoto JG, Duker JS. In vivo measurement of retinal physiology with high-speed ultrahigh-resolution optical coherence tomography. *Opt Lett*. 2006;31:2308–2310.
9. Yao X, George J. Near-infrared imaging of fast intrinsic optical responses in visible light-activated amphibian retina. *J Biomed Opt*. 2006;11:064030.
10. Jonnal RS, Rha J, Zhang Y, Cense B, Gao W, Miller DT. *In vivo* functional imaging of human cone photoreceptors. *Opt Express.* 2007;15:16141–16160.
11. Romero-Borja F, Venkateswaran K, Roorda A, Hebert TJ. Optical slicing of human retinal tissue in vivo with the adaptive optics scanning laser ophthalmoscope. *Appl Opt*. 2005;44:4032–4040.
12. Mulligan JB, MacLeod DIA. In search of an optoretinogram. In: *Vision Science and Its Applications (Technical Digest Series, vol. 2)*. Washington, DC: Optical Society of America; 1994:167–170.
13. Roorda A, Romero-Borja F, Donnelly W, Queener H, Hebert T, Campbell M. Adaptive optics scanning laser ophthalmoscopy. *Opt Express*. 2002;10:405–412.
14. Poonja S, Patel S, Henry L, Roorda A. Dynamic visual stimulus presentation in an adaptive optics scanning laser ophthalmoscope. *J Refractive Surg*. 2005;21:575–580.
15. Grieve K, Tiruveedhula P, Zhang Y, Roorda A. Multi-wavelength imaging with the adaptive optics scanning laser ophthalmoscope. *Opt Express*. 2006;14:12230–12242.
16. Stockman A, Sharpe LT. The spectral sensitivities of the middle- and long-wavelength-sensitive cones derived from measurements in observers of known genotype. *Vis Res*. 2000;40:1711–1737.
17. Roorda A, Williams D. The arrangement of the three cone classes in the living human eye. *Nature*. 1999;397:520–522.
18. *ANSI, American National Standard for the Safe Use of Lasers*. ANSI Z136 1–2000. Orlando, FL: Laser Institute of America; 2000.
19. Curcio CA, Sloan KR, Kalina RE, Hendrickson AE. Human photoreceptor topography. *J Comp Neurol*. 1990;292:497–523.
20. Vogel CR, Arathorn DW, Roorda A, Parker A. Retinal motion estimation in adaptive optics scanning laser ophthalmoscopy. *Opt Express*. 2006;14:487–497.
21. Stevenson SB, Roorda A. Correcting for miniature eye movements in high resolution scanning laser ophthalmoscopy. *Proc SPIE*. 2005;5688A:145–151.
22. Boycott BB, Dowling JE. Organisation of the primate retina: light microscopy. *Phil Trans R Soc Lond B Biol Sci*. 1969;255:109–184.
23. Shahidi M, Wang Z, Zelkha R. Quantitative thickness measurement of retinal layers imaged by optical coherence tomography. *Am J Ophthalmol*. 2005;139:1056–1061.
24. Rushton WAH, Henry GH. Bleaching and regeneration of cone pigments in man. *Vision Res*. 1968;8:617–631.